KMAN PUBLISHING INSTITUTE

Article history:
Received 04 October 2025
Revised 24 January 2026
Accepted 28 January 2026
Published online 01 March 2026

Journal of Resource Management and Decision Engineering

Volume 5, Issue 2, pp 1-15

An Engineering and Management Approach to Optimizing the Behavior of Strip Footings on Geocell-Reinforced Saturated Sand: Analyzing the Effect of Embedment Depth, Reinforcement Width, and Geocell Geometry

Manesht. Maleki Vasegh[1], Vahid. Rostami[2*], Hamidreza. Rabieefar[3]

[1] Department of Civil Engineering, Ki.C., Islamic Azad University, Kish, Iran.
[2] Department of Civil Engineering, Ha.C., Islamic Azad University, Hamedan, Iran.
[3] Department of Civil Engineering, STB., Islamic Azad University, Tehran, Iran.

*** Corresponding author email address**: rostami.vahid@iau.ac.ir

A r t i c l e I n f o

Article type:
Original Research

How to cite this article:
Maleki Vasegh, M., Rostami, V. & Rabieefar, H. (2026). An Engineering and Management Approach to Optimizing the Behavior of Strip Footings on Geocell-Reinforced Saturated Sand: Analyzing the Effect of Embedment Depth, Reinforcement Width, and Geocell Geometry. *Journal of Resource Management and Decision Engineering, 5*(2), 1-15.
https://doi.org/10.61838/kman.jrmde.5.2.245

A B S T R A C T

Improving the performance of shallow foundations on problematic soils such as saturated sand requires integrating precise engineering design with informed management of influential parameters. This research examines geocell systems from an engineering-management perspective to provide solutions that simultaneously enhance bearing capacity and optimize economic and executional efficiency. In a systematic laboratory study, the effect of three key parameters with engineering significance (embedment depth, reinforcement width, and geocell geometry) on the behavior of a strip footing on saturated sand was investigated. These parameters were considered as design management variables to quantify their impact on the system's performance and economic indicators. Forty-nine tests were conducted, including an unreinforced reference case, under uniform loading. The results showed that optimal management of embedment depth at shallow depths (u/B = 0.25) combined with engineered selection of reinforcement width (L/B ≥ 3) can increase the Bearing Capacity Ratio (BCR) up to 4.2 times. From the perspective of material management and technical selection, geocells with greater height and smaller cell aperture (G3) were identified as the superior engineering option. This study demonstrates that through engineering design based on testing and intelligent management of effective parameters, reinforced systems can be achieved that are both technically efficient and economically and executionally optimal. The findings provide a framework for managerial decision-making in selecting configuration, materials, and execution methods in real-world projects.

Keywords: *Geocell Reinforcement; Saturated Sand; Strip Footing; Bearing Capacity Ratio (BCR); Load–Settlement Behavior; Embedment Depth and Reinforcement Width*

1. Introduction

Soil stability is a fundamental concern in the design of shallow foundations, because most natural soils possess very low tensile strength and limited shear resistance, which can lead to low bearing capacity, excessive settlements and lateral spreading under service and ultimate loads (Tianzheng et al., 2023; Wang et al., 2023). Classical bearing capacity theories assume homogeneous, unreinforced ground and often require conservative design factors to account for these shortcomings (Chen et al., 2025; Terzaghi, 1943). To overcome these limitations, various ground-improvement techniques have been developed, including densification, chemical stabilisation and reinforced soil systems. Among these, reinforcement with polymeric inclusions has proved particularly attractive because it can be installed with relatively low cost and minimal construction time while providing substantial gains in strength and stiffness (Binquet & Lee, 1975; Chen & Abu-Farsakh, 2015; Fragaszy & Lawton, 1984).

The concept of reinforcing soil with tensile elements, first formalised in the context of "reinforced earth" and later extended to geosynthetics, has been validated by numerous model and full-scale tests on planar (two-dimensional) reinforcement beneath shallow foundations (Binquet & Lee, 1975; Fragaszy & Lawton, 1984; Huang & Tatsuoka, 1990). Early works on reinforced earth slabs and sand subgrades showed that strips or sheets of reinforcement placed at suitable depths could increase the ultimate bearing capacity by factors of about 1.5–3.0, depending on the number of layers, length and embedment depth (Binquet & Lee, 1975; Fragaszy & Lawton, 1984). More detailed parametric studies on strip footings on geogrid-reinforced sand demonstrated that the improvement depends strongly on reinforcement length and spacing and that an optimum reinforcement zone exists within about 1.0–2.0 footing widths below the base (Huang & Tatsuoka, 1990; Shin & Das, 2000). These studies provided the basis for current design approaches for geosynthetic-reinforced foundations and highlighted the role of reinforcement in altering failure mechanisms and spreading loads over a wider influence area (Chen & Abu-Farsakh, 2015; Huang & Tatsuoka, 1990).

Despite these advances, planar reinforcement systems primarily mobilise tensile resistance along relatively thin inclusion layers and provide limited three-dimensional confinement to the surrounding soil. Geocells—three-dimensional honeycomb-like geosynthetic mattresses—were introduced to address this limitation by confining the infill soil within interconnected cells and mobilising hoop tension and bending resistance in the cell walls. Model tests on strip footings supported on geocell-reinforced sand have shown that, at optimum combinations of geocell height (h/B), width (L/B) and embedment depth (u/B), the ultimate bearing capacity can increase by factors of about 3–8 compared with unreinforced sand, with substantial reductions in settlement at design load levels (Dash et al., 2001a, 2001b). For example, Dash et al. (Dash et al., 2001a) reported bearing capacity ratios (BCR) of up to about 4 for strip footings on geocell-reinforced sand, while the addition of a planar geogrid layer beneath the geocell mattress produced further gains in capacity and reduced surface heave (Dash et al., 2001b).

Subsequent experimental and numerical studies have clarified the mechanisms and efficiency of geocell reinforcement for shallow foundations. Moghaddas Tafreshi and Dawson (Moghaddas Tafreshi & Dawson, 2010) compared a strip footing on geocell-reinforced sand with an equivalent planar geotextile system using the same amount of reinforcement material and showed that at a settlement level of 4% the geocell increased the bearing capacity by a factor of 2.73 and reduced settlement by 63%, whereas planar reinforcement achieved an improvement factor of 1.88 and a 47% reduction in settlement. Pokharel et al. (Pokharel et al., 2010) demonstrated that a single geocell under a loading plate could increase the stiffness of the base by about 50% and the ultimate load by up to 100% relative to an unreinforced base, with performance strongly influenced by cell height, shape and stiffness. Parametric work on geocell-reinforced sand foundations has further shown that increasing the geocell height and reinforcement width, and selecting an appropriate cell geometry, leads to higher BCR and lower settlements, although with diminishing returns beyond certain thresholds of h/B and L/B (Dash, 2010; Moghaddas Tafreshi & Dawson, 2010; Najjar et al., 2025; Pokharel et al., 2010).

Most of the above investigations, however, have been carried out on dry or partially saturated sand. Under saturated conditions, the presence of pore water reduces effective stress and may induce apparent cohesion effects, significantly altering the bearing capacity and settlement response of both unreinforced and reinforced ground. Recent work on saturated reinforced sandy ground has shown that saturation can markedly reduce the ultimate bearing capacity compared with dry conditions and modifies the mobilisation of reinforcement forces at failure (Huang, 2016). Although the beneficial effect of reinforcement is preserved, the

magnitude of improvement and the optimum reinforcement layout may differ from those in dry sand. Systematic experimental data on geocell-reinforced saturated sand supporting strip footings remain relatively scarce, particularly for combined variations of geocell height, aperture size, reinforcement width and embedment depth.

The present study aims to address this gap by performing a comprehensive small-scale model test program on a strip footing resting on saturated, poorly graded sand reinforced with geocell mattresses. Four geocell configurations with different cell heights and aperture sizes are examined, in conjunction with several reinforcement widths (L/B) and embedment depths (u/B). The load–settlement response is used to determine the ultimate bearing capacity and to quantify performance in terms of the bearing capacity ratio (BCR) between reinforced and unreinforced conditions. By systematically exploring the influence of geocell geometry and placement on the behaviour of strip footings on saturated sand, the study seeks to (i) identify practically relevant optimum ranges of u/B, L/B, h/B and aperture size for geocell reinforcement, and (ii) provide experimental evidence that can support the development and calibration of design methods for foundations on geocell-reinforced saturated sandy soils.

2. Materials and Experimental Setup

2.1. Foundation soil

The soil used in this study is a clean siliceous sand classified as poorly graded sand (SP) according to the Unified Soil Classification System (USCS) and parameters are summarized in Table 1.

Table 1

Soil properties

Soil type	Unit weight	Frictional degree Φ	Cohesion
Sand	1.32 (gr/cm^3)	28	0

The grain-size distribution curve of the sand, obtained from standard sieve analysis, indicates a relatively uniform gradation consistent with the SP classification and is presented in Figure 1.

Figure 1

Grain-size distribution of the sand

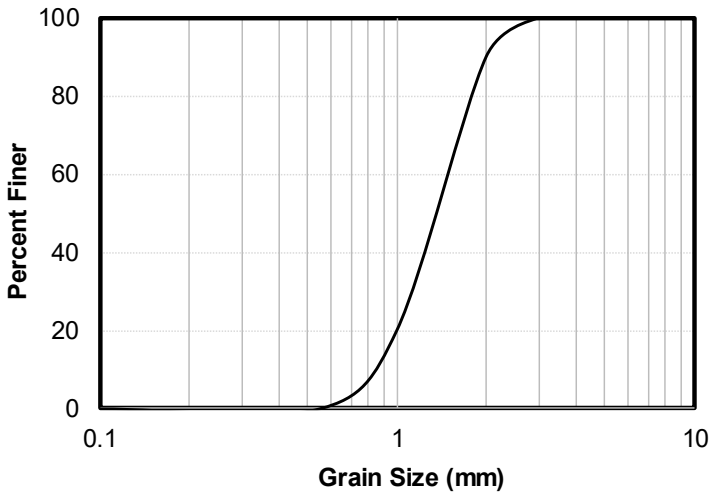

2.2. Geocell Reinforcement

2.2.1. Geogrid Material

The soil bed was reinforced using geocell layers fabricated from commercial polymeric geogrid sheets (Rockshield®). The geogrid sheets were cut and bonded along selected lines to create a three-dimensional geocell mattress following the procedure proposed by Dash et al shown in Figure 2, and the mechanical properties of the geogrid are given in Table 2.

Table 2

Geogrid properties

Brand	Rockshild R.S.B 161
Material	HDPE
Mesh Aperture	10*10 mm
Height Weight	700 gr/m^2
Thickness	3.6 mm
Working Temp	-50/+85c
Tensile Strength	26.2 MPa

Figure 2

Photograph of the geogrid used to make the geocell

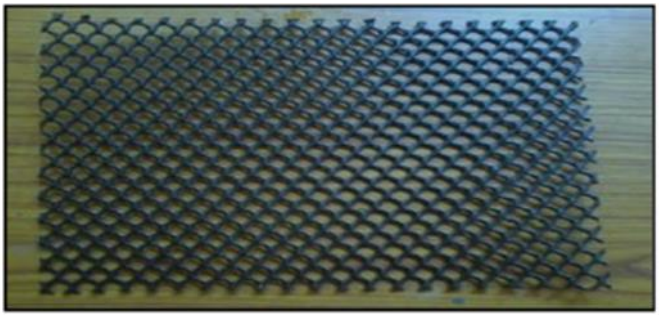

2.2.2. Geocell Configuration

Four different geocell configurations, denoted G1–G4, were prepared by combining two cell heights and two aperture sizes shown in figure 3. In terms of the model footing width B, two height ratios (h/B = 0.5 and 1.0) and two relative aperture sizes were considered, leading to four distinct geocell types. Each geocell mattress extended laterally beyond the footing edges; the width of reinforcement L was varied such that L/B = 2, 3 and 5 in the test program. The geometry of geocell types given in Table 3.

Figure 3

Geocell mattress used in the laboratory tests

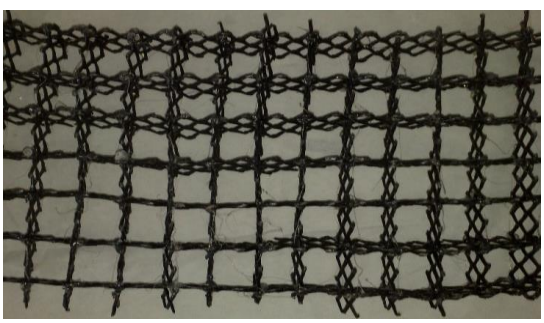

Table 3

The geometry of Geocell types

Geocell type	h	z
G1	B	B
G2	0.5B	B
G3	B	0.5B
G4	0.5B	0.5B

2.3. *Model footing and Test Tank*

The model foundation was a rigid strip footing simulated by a steel plate with width B and a length much larger than its width (length/width > 5), so that plane strain conditions could be approximated in the central region underneath the footing. Based on the test settlement level of 30% of the footing width corresponding to 15 mm, the footing width B is 50 mm in the model tests.

All experiments were performed in a rigid steel tank with internal dimensions 0.50 m × 0.50 m × 0.50 m (length × width × height). Because the tests were carried out on saturated sand, a drainage valve was installed at the bottom of the tank. The tank height was chosen based on Boussinesq's stress distribution solution: for a strip footing, the additional vertical stress at depths greater than about 4B is less than 10–11% of the stress immediately beneath the footing. To avoid any boundary influence from the rigid base, the tank height was set to approximately 0.51 m, i.e. slightly larger than 4B, while the thickness of the sand layer in the tests was 25 cm. The main geometrical parameters of the physical model—footing width B, geocell width L, geocell height h, geocell mesh size z, distance of the geocell layer from the footing base u—are illustrated schematically in Figure 4.

Figure 4

Cross-sectional view of the model test setup

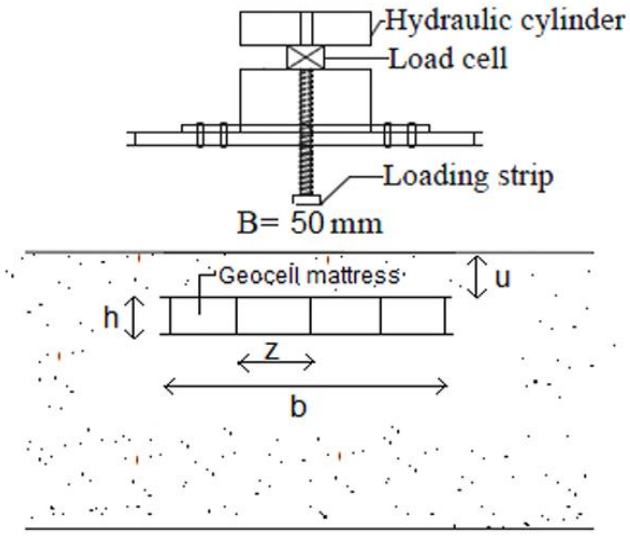

2.4. *Loading System and Instrumentation*

A small-scale loading frame was specifically designed and fabricated to apply vertical loads to the model footing placed on the sand bed. The general configuration of this apparatus is shown in Figure 5. The main components are:

(i) the rigid steel tank acting as the soil container;

(ii) a vertical loading system consisting of a mechanical jack mounted on a steel frame; and

(iii) a load–settlement measurement system.

Figure 5

Cross-section of the model in the test tank

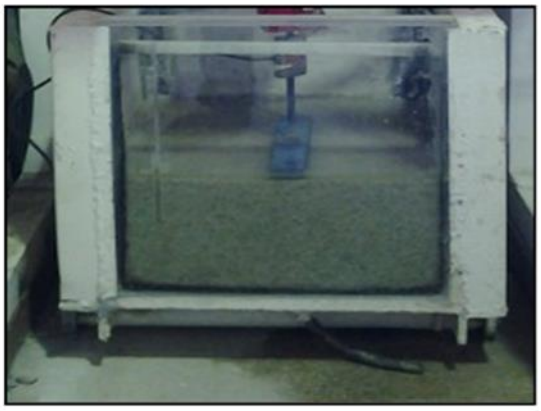

Figure 6

Schematic view of the loading apparatus

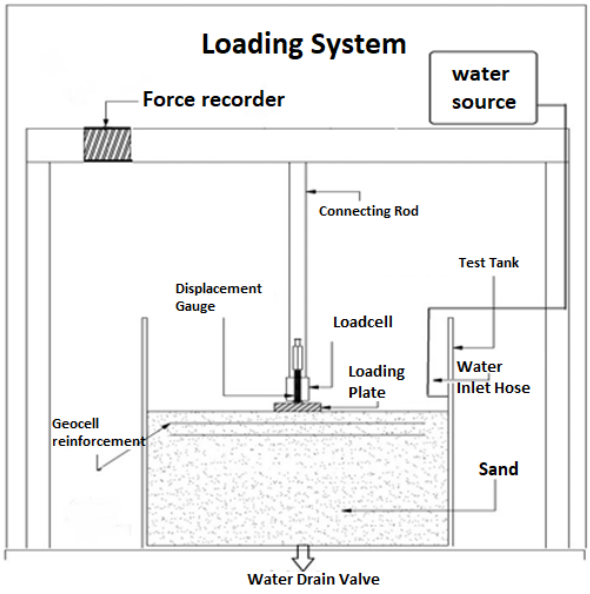

The vertical load transmitted to the footing was measured using a load cell connected between the jack and the model footing. The footing settlement was monitored by a dial gauge or linear displacement transducer mounted vertically on top of the footing plate. The data acquisition system used to record the applied load shown in figure 6.

2.5. Sample Preparation and Saturation Procedure

Before placing the reinforcement and footing, the sand bed was prepared in the tank using a controlled raining method in order to obtain a homogeneous deposit. The sand was poured from a specified height to achieve the target unit weight, and the procedure was repeated in several layers until the desired thickness (H = 25 cm) was reached. For the reinforced tests, the geocell mattress was placed at the desired embedment depth u from the footing base, then backfilled and compacted with sand inside and above the cells according to the same raining procedure.

After preparation in dry condition, the sand bed was saturated by allowing water to infiltrate slowly from the top surface through small perforations, so that no additional hydraulic gradients or disturbance were induced in the soil layers. The water level was carefully raised and the specimen

was left for a sufficient time to ensure full saturation. During all model preparations, efforts were made to keep the unit weight of the sand as constant as possible for all tests.

After the completion of saturation, the footing plate was placed on the surface of the sand bed (or on a shallow trench when required by the test configuration), and the displacement gauge was attached vertically on the footing. The load was then applied monotonically at a constant rate of approximately 1 mm/min until a settlement equal to 30% of the footing width (s/B = 0.3) was reached. The applied load and corresponding settlement were recorded simultaneously throughout each test.

2.6. Test Program

The experimental program consisted of one test on an unreinforced saturated sand bed and 48 tests on geocell-reinforced beds. In the reinforced tests, four geocell types (G1–G4) were investigated. For each geocell type, the embedment depth was varied such that u/B = 0.25, 0.50, 0.75 and 1.0, and the reinforcement width was taken as L/B = 2, 3 and 5, resulting in 12 tests per geocell type (Table 3). Thus, a total of 49 loading tests were carried out in this study given in table 4.

Table 4

Summary of the laboratory test program and main dimensionless parameters.

Test series	Type of reinforcement	u/B	b/B	No. of the tests
0	Unreinforced	…….	……	1
1	Geocell reinforced (type G1)	0.25, 0.5, 0.75, 1	2,3,5	12
2	Geocell reinforced (type G2)	0.25, 0.5, 0.75, 1	2,3,5	12
3	Geocell reinforced (type G3)	0.25, 0.5, 0.75, 1	2,3,5	12
4	Geocell reinforced (type G4)	0.25, 0.5, 0.75, 1	2,3,5	12

3. Results and Discussion

A total of 49 plate load tests were carried out on the strip footing, including one test on an unreinforced saturated sand bed and 48 tests on sand beds reinforced with different geocell configurations, embedment depths and reinforcement widths.

To compare the performance of the various configurations in a consistent way, the bearing pressure corresponding to a settlement ratio of s/B=0.3s/B = 0.3s/B=0.3 was adopted as the reference value in all tests. The improvement due to reinforcement is expressed in terms of the bearing capacity ratio (BCR), defined as:

$$BCR = \frac{q_r}{q_{un}}$$

where $q_r$is the ultimate bearing pressure of the geocell-reinforced sand and q_{un} is the corresponding bearing pressure for the unreinforced sand at the same settlement ratio. The variations of BCR with geocell embedment depth, reinforcement width and geocell geometry are presented in the following subsections.

3.1. Effect of Geocell Embedment Depth (u/B)

Figure 7(a)–(d) present the load–settlement (q–ε) curves for the strip footing on saturated sand reinforced with geocell types G1, G2, G3 and G4, respectively, for a constant reinforcement width L/B = 2 and four embedment depths u/B = 0.25, 0.50, 0.75 and 1.0, together with the unreinforced case. In all four figures, the unreinforced curve has the lowest stiffness and ultimate bearing capacity; ε reaches about 0.30 at comparatively low stress levels, reflecting the limited confinement and absence of tensile reinforcement in the saturated sand. For each geocell type, all reinforced curves lie clearly to the right of the unreinforced curve, indicating that the geocell layer substantially increases the mobilized stress at any given settlement. The effect of embedment depth is systematic: the shallowest placement, u/B = 0.25, consistently produces the stiffest response and the highest ultimate stress, while deeper placements (u/B = 0.50, 0.75 and 1.0) exhibit progressively softer responses and reduced capacities. At u/B = 1.0, the reinforced and unreinforced curves are much closer, showing that the influence of the reinforcement becomes limited when the geocell is located well below the primary shear zone beneath the footing.

Figure 7

Load–settlement curves for G1–G4 (L/B = 2) at various embedment depths (u/B = 0.25–1.0), and the unreinforced case.

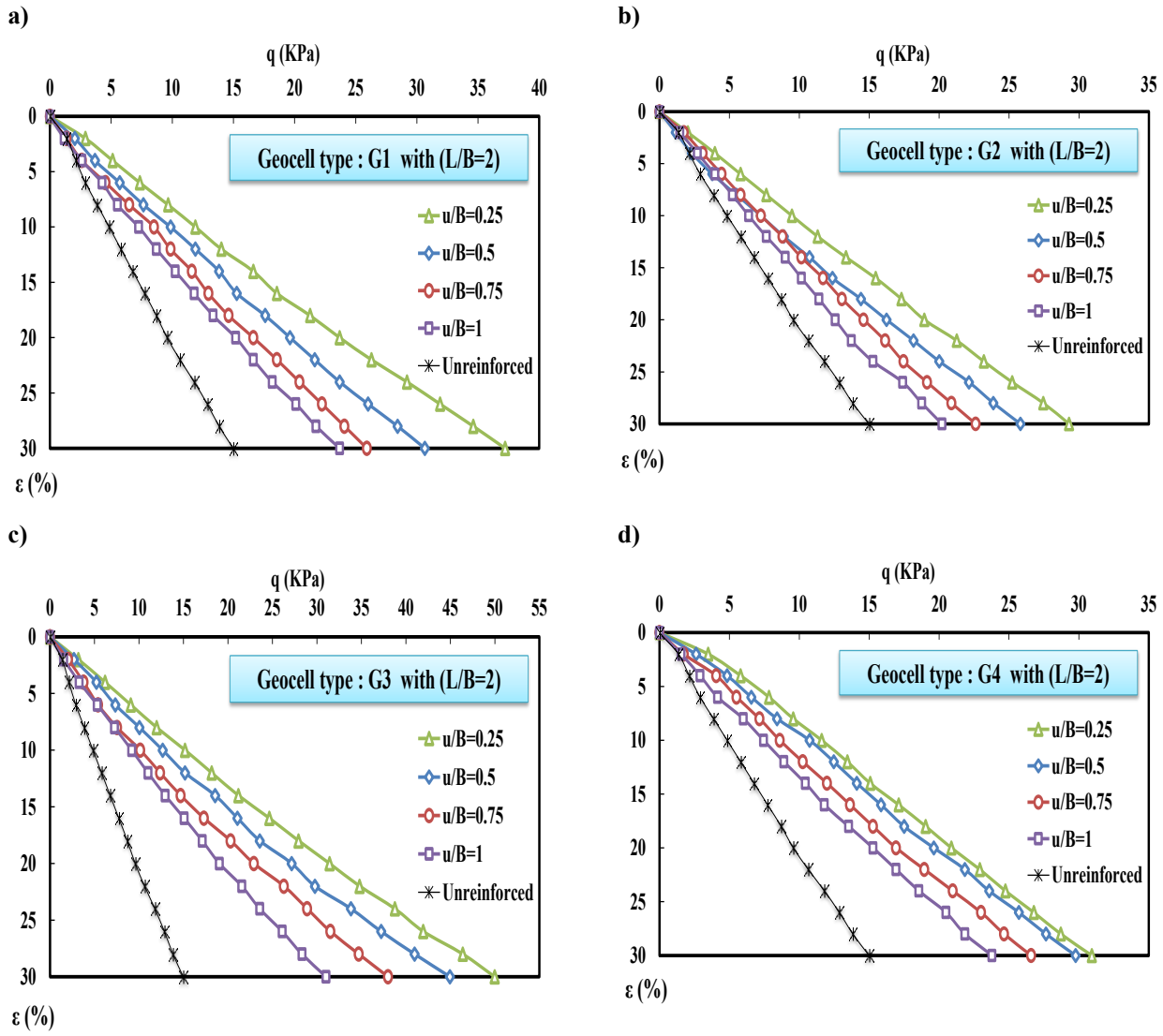

The corresponding variation of BCR with embedment depth is shown in Figure 8 for geocell types G1–G4 and reinforcement widths L/B = 2, 3 and 5. For all geocell configurations, the maximum BCR occurs at u/B = 0.25, confirming that the reinforcement is most effective when placed close to the footing base. At this shallow depth, typical BCR values range from about 2.6–3.1 for G1, 1.8–2.1 for G2, 3.6–4.2 for G3 and 2.5–2.9 for G4, depending on L/B (Figure 8). As u/B increases, BCR decreases monotonically for every geocell type and reinforcement width. At u/B = 1.0, the BCR falls to roughly 1.4–1.7 for G1, 1.2–1.4 for G2, 2.0–2.4 for G3 and 1.3–1.6 for G4, indicating that when the geocell is placed away from the active shear zone its contribution to the load–carrying mechanism is significantly reduced. These trends can be explained by the increasing thickness of unreinforced sand above the geocell at larger u/B: this upper layer undergoes most of the deformation before the reinforcement is mobilised, leading to larger settlements at lower stresses and a lower overall BCR. Among the four geocell types, G3 consistently provides the highest BCR values over the whole range of u/B and L/B, followed by G1, G4 and G2, highlighting the importance of geocell geometry in governing confinement efficiency and bearing capacity.

Figure 8

BCR–u/B variation for G1–G4 at L/B = 2–5, at different u/B.

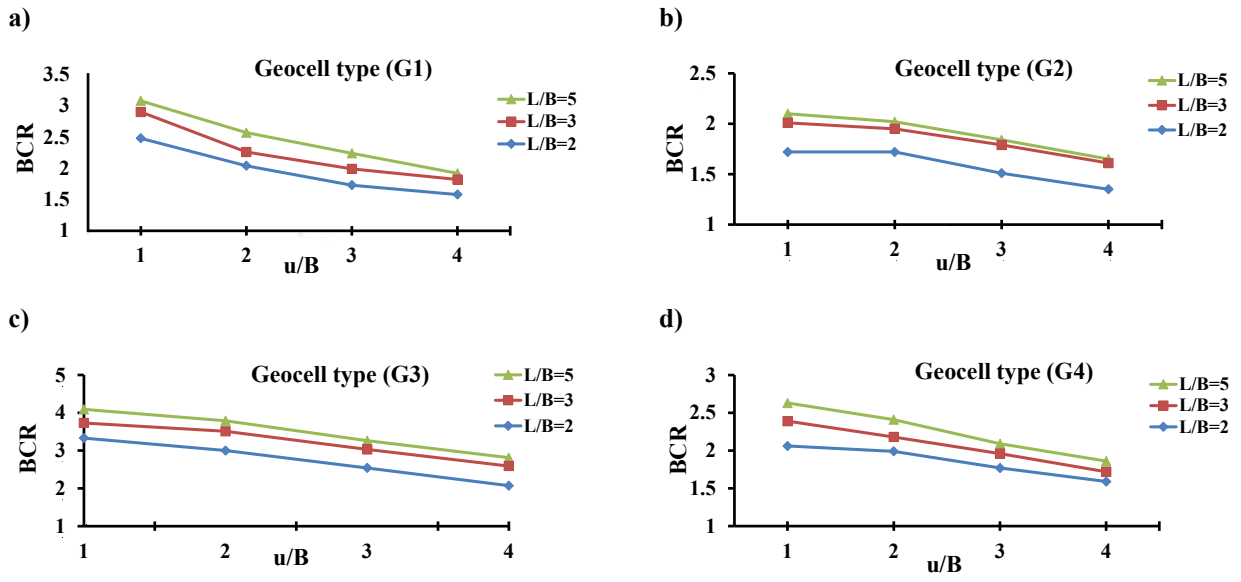

3.2. *Effect of Reinforcement Width (L/B)*

The influence of reinforcement width on the footing response is illustrated in Figure 9(a)–(d), which show the load–settlement (q–ε) curves for geocell type G1 at different embedment depths (u/B = 0.25, 0.50, 0.75 and 1.0) and reinforcement widths (L/B = 2, 3 and 5), together with the unreinforced case. In all four subfigures, the unreinforced footing again exhibits the lowest stiffness and capacity, and the reinforced curves lie to the right of the unreinforced curve. At each embedment depth, increasing L/B from 2 to 3 and 5 systematically shifts the reinforced curves further to the right, indicating that wider geocell mattresses enable higher stresses to be mobilized at the same settlement.

Figure 9

Load–settlement curves for G1-reinforced sand at various embedment depths (u/B = 0.25–1.0) and widths (L/B = 2–5), and the unreinforced case.

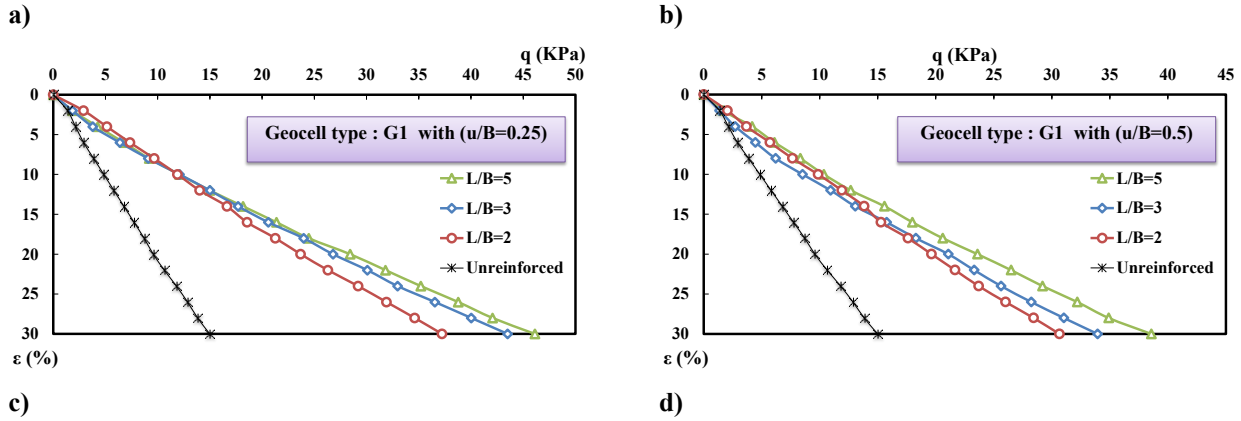

c)

d)

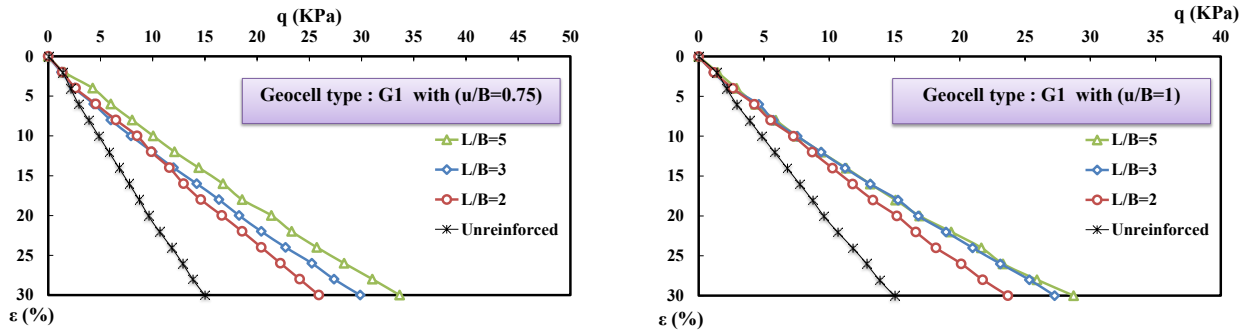

The effect of width is most pronounced at the shallowest embedment depth, u/B = 0.25 (Figure 9(a)), where the geocell lies directly within the main shear zone. In this case, the curve for L/B = 2 is closest to the unreinforced response, while the curves for L/B = 3 and L/B = 5 show progressively higher stresses over the entire settlement range; the separation between the widths becomes more significant at medium to large settlements near ε ≈ 0.30. At u/B = 0.50 (Figure 9(b)), the same ordering of curves is observed, but the distance between the L/B = 3 and L/B = 5 curves is smaller, indicating a reduced marginal gain from further increasing the width. At u/B = 0.75 and 1.0 (Figures 9(c) and 9(d)), all reinforced curves still outperform the unreinforced case, but the three reinforced curves are closer together, showing that the sensitivity to L/B diminishes as the geocell is placed deeper and a thicker unreinforced sand layer deforms above it.

Figure 10

BCR–u/B variation for G1 at L/B = 2–5 and different u/B.

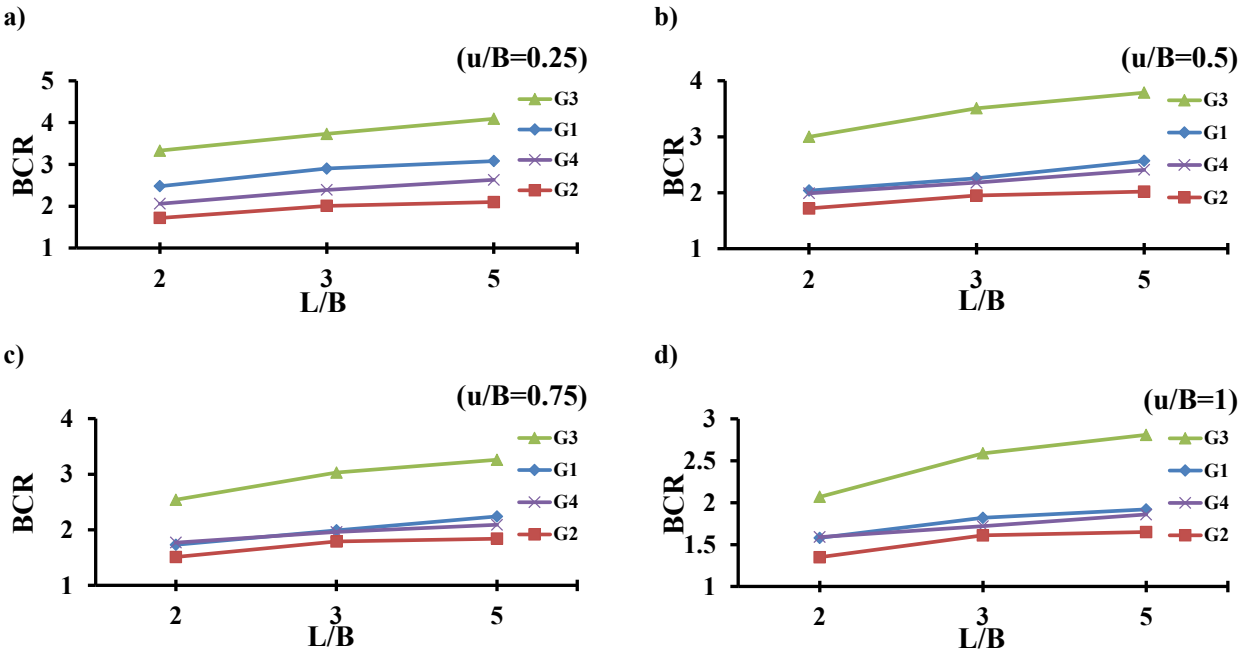

The corresponding trends in terms of BCR are summarised in Figure 10, which presents the BCR for G1 as a function of u/B for different reinforcement widths L/B = 2, 3 and 5. For any given u/B, BCR increases with L/B, confirming that wider reinforcement provides a larger confinement zone and engages a greater volume of soil. At u/B = 0.25, for example, increasing L/B from 2 to 5 raises the BCR for G1 from about 2.6 to 3.1 (Figure 10), representing a substantial improvement in bearing capacity. At greater embedment depths, the same trend persists but the incremental benefit of increasing width is smaller; by u/B = 1.0 the BCR curves for L/B = 2, 3 and 5 converge, indicating

that only a limited portion of the reinforcement participates in the failure mechanism when it is located far below the footing. Overall, the results suggest that extending the geocell layer laterally is beneficial up to several footing widths, but that most of the improvement is achieved once L/B ≈ 3 is reached, with additional widening to L/B = 5 giving more modest gains.

3.3. *Effect of Geocell Geometry and Type*

This section examines the influence of geocell geometry on the behaviour of the reinforced foundation by considering two key parameters: the geocell height (h/B) and the aperture size (z/B). The four geocell types used in the experiments represent different combinations of these parameters. To isolate the effect of each, geocell pairs with identical aperture size but different heights (G1 vs. G2) and with identical height but different aperture sizes (G1 vs. G3, G2 vs. G4) are compared in terms of q–ε response and BCR.

3.3.1. *Effect of Geocell Height (h/B)*

Figures 11(a)–(c) show the load–settlement (q–ε) curves for geocell types G1 (h/B = 1.0) and G2 (h/B = 0.5) at u/B = 0.25 for reinforcement widths L/B = 2, 3 and 5, together with the unreinforced footing. For each width, both reinforced curves lie to the right of the unreinforced curve, confirming the beneficial effect of geocell inclusion. Moreover, for a given L/B, the G1 curve (taller geocell) is consistently to the right of the G2 curve over almost the entire settlement range, indicating that increasing the cell height enhances both the initial stiffness and the ultimate load. The difference between G1 and G2 becomes more pronounced as L/B increases and at larger settlements, where the reinforcement is more fully mobilized.

Figure 11

Load–settlement curves for G1 and G2 at u/B = 0.25 and L/B = 2, 3, 5.

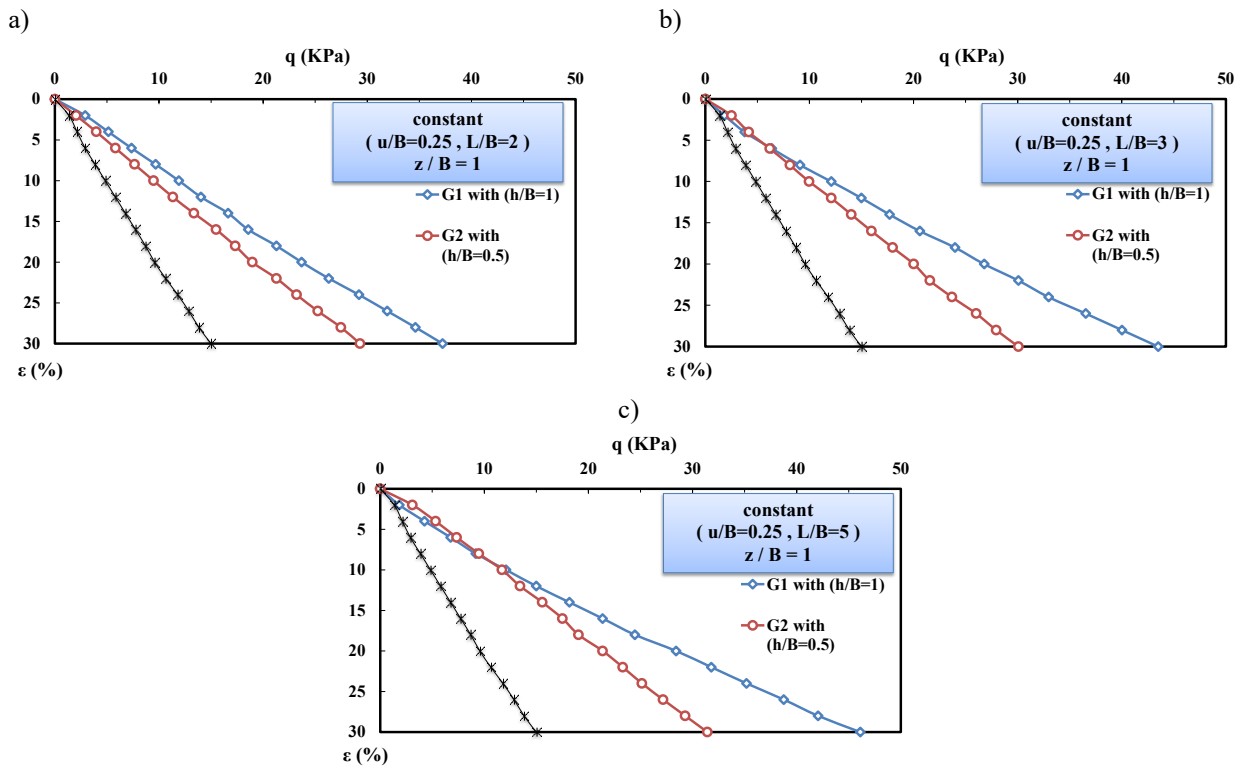

The quantitative influence of geocell height is depicted in Figure 12, which presents BCR values for G1 and G2 as a function of u/B at L/B = 2, 3 and 5. At u/B = 0.25, increasing h/B from 0.5 (G2) to 1.0 (G1) raises BCR from about 1.7 to 2.5 for L/B = 2, from about 2.0 to 2.9 for L/B = 3, and from approximately 2.1 to 3.1 for L/B = 5 (Figure 12). These increases correspond to improvements on the order of 35–50%. At greater embedment depths (u/B = 0.50–1.0), the absolute BCR values are lower for both geocell types, but the taller geocell still provides gains of roughly 10–25% for

all reinforcement widths. These trends indicate that taller geocells confine a thicker sand layer and allow greater mobilisation of membrane and bending actions within the mattress, so that a larger volume of soil participates in the reinforced zone and the composite soil–geocell system behaves more like a stiff beam or slab beneath the footing.

Figure 12

BCR variation with geocell height (h/B = 0.5 for G2, h/B = 1.0 for G1) at z/B = 1 and L/B = 2, 3 and 5.

a) b)

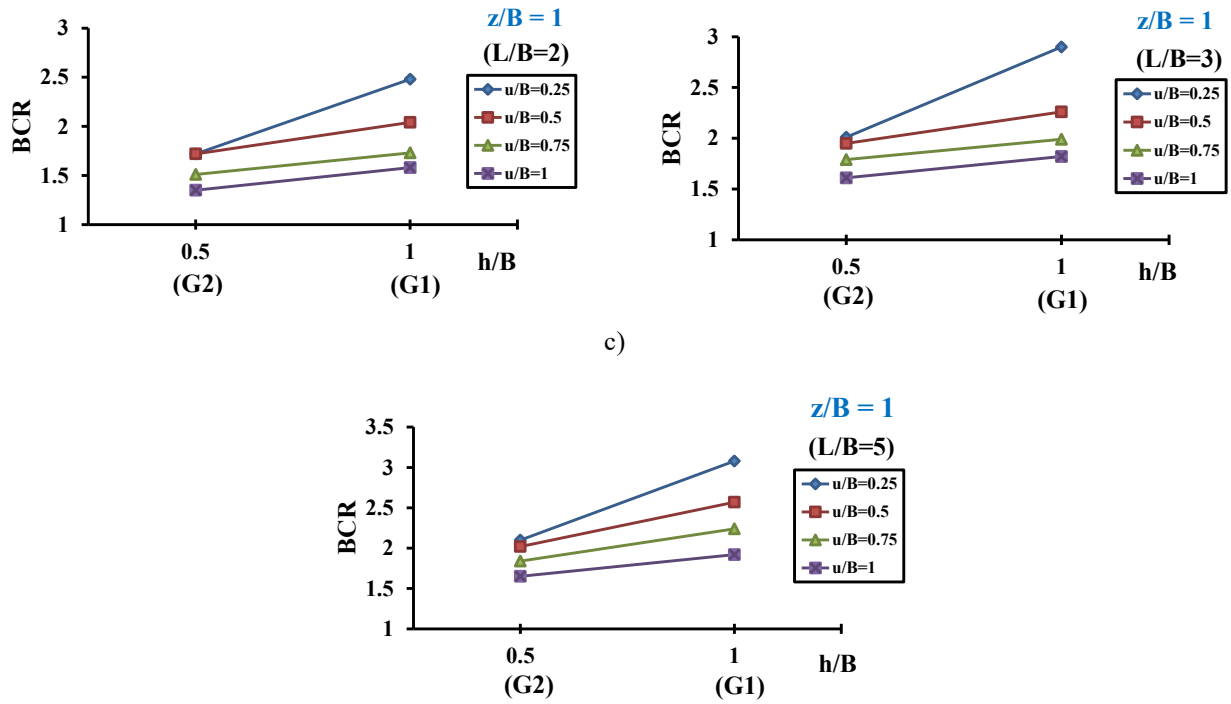

c)

3.3.2. *Effect of Geocell Aperture Size (z/B)*

The effect of aperture size is investigated by comparing geocell types with the same height but different cell openings. Figures 13(a)–(c) present the q–ε curves for G1 (z/B = 1.0) and G3 (z/B = 0.5) at u/B = 0.25 for L/B = 2, 3 and 5, together with the unreinforced case.

Figure 13

Load–settlement curves for G1 and G3 at u/B = 0.25 and L/B = 2, 3, 5.

a) b)

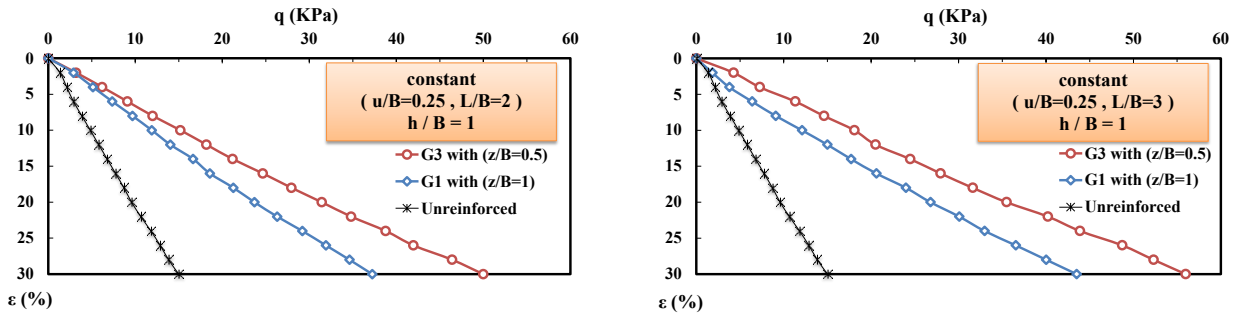

c)

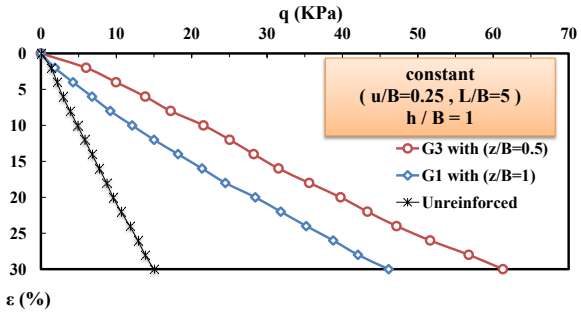

For each reinforcement width, both geocell types improve the footing response relative to the unreinforced sand, but the curves for G3 (smaller aperture) lie consistently to the right of those for G1, showing that the smaller-aperture geocell mobilizes higher stresses at the same settlement. The difference between G1 and G3 becomes more marked as L/B increases and at larger settlements, where the confining effect of the geocell is more fully engaged.

Figure 14

BCR variation with geocell aperture ratio (z/B = 0.5 for G3, h/B = 1 for G1) at h/B = 1 and L/B = 2, 3 and 5.

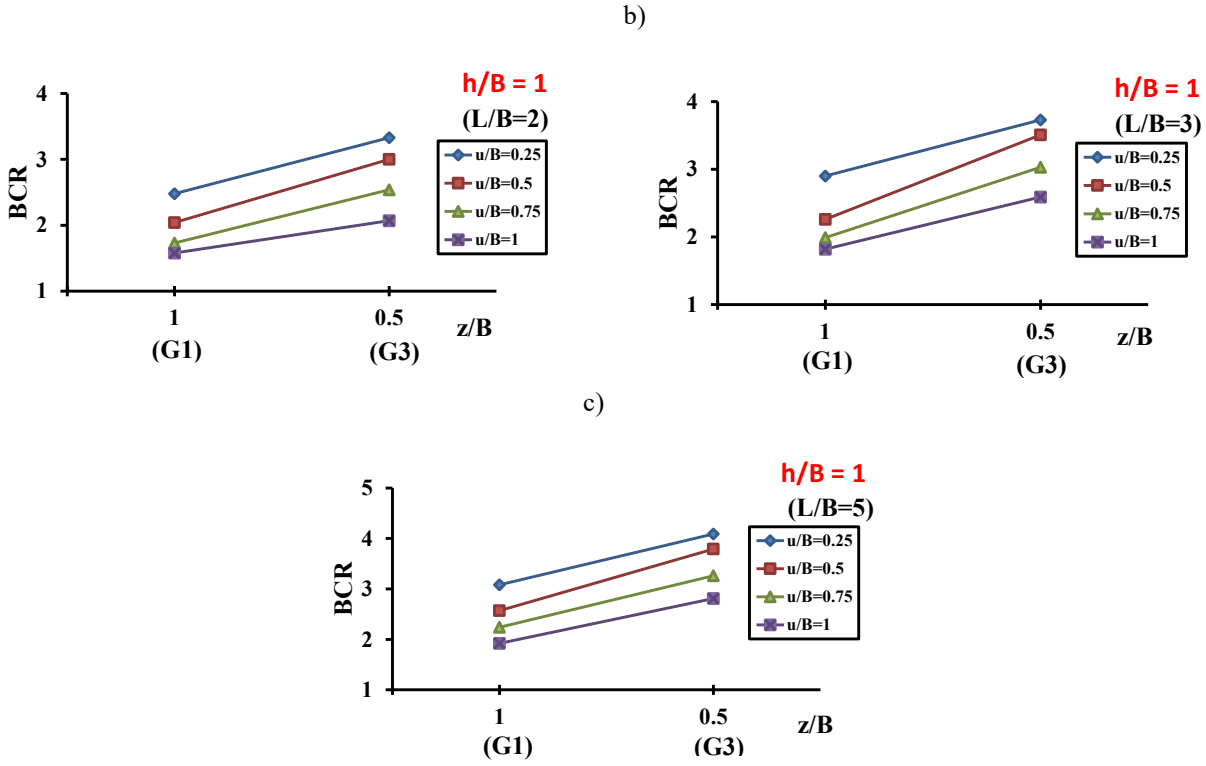

Figure 14 shows the corresponding BCR values for G1 and G3 at h/B = 1.0 and L/B = 2, 3 and 5 as a function of u/B. At u/B = 0.25 and L/B = 2, the BCR increases from about 2.5 for G1 to around 3.3 for G3; at L/B = 5, the BCR increases from approximately 3.1 to 4.1 (Figure 14). Similar, though slightly smaller, improvements are observed at u/B = 0.50 and 1.0. In all cases, G3 yields higher BCR values than G1 over the full range of depths and widths considered. These results demonstrate that reducing the aperture size enhances lateral confinement and soil–geocell interlocking, thereby increasing the mobilized shear resistance within the reinforced zone and significantly improving the bearing capacity. When combined with a relatively large height and adequate width, as in the G3 configuration at u/B = 0.25 and L/B = 5, the small-aperture geocell provides the best overall performance among the tested systems.

3.4. *Settlement Reduction*

Although the performance has been quantified primarily in terms of BCR at ε = 0.30, the q–ε curves in Figures 7, 9, 11 and 13 also show that geocell reinforcement leads to substantial settlement reduction at working stress levels. For a given applied pressure, the reinforced foundations exhibit smaller settlements and smoother post-peak behavior than the unreinforced footing, particularly for configurations combining shallow embedment (u/B ≈ 0.25), larger reinforcement widths (L/B ≥ 3) and favorable geocell geometries (taller cells with smaller apertures). Under these conditions, the geocell mattress acts as a stiffened load-distribution layer, limiting vertical compression and lateral spreading of the saturated sand and thereby improving both ultimate capacity and serviceability performance of the footing.

4. Conclusion

This experimental study has examined the behavior of a strip footing on saturated sand reinforced with geocell layers through a systematic program of 49 model tests. Four geocell types (G1–G4), representing different combinations of cell height and aperture size, were investigated over a range of embedment depths (u/B = 0.25–1.0) and reinforcement widths (L/B = 2–5). The results consistently showed that geocell inclusion markedly improves the load–settlement response compared with the unreinforced condition: for the best configuration, the bearing capacity ratio (BCR) reached values of about 4.0–4.2, indicating an increase in ultimate capacity of up to four times, together with a significant reduction in settlement at working stress levels.

The depth of placement of the geocell layer was identified as a primary factor controlling performance. For all geocell types and widths, the maximum BCR was obtained when the reinforcement was placed at a shallow depth of u/B ≈ 0.25, where the geocell intersects the principal shear zone beneath the footing and its confinement and membrane actions are fully mobilised. As the embedment depth increased to u/B = 0.50, 0.75 and 1.0, BCR values decreased monotonically, reflecting the greater thickness of unreinforced sand above the geocell and the associated increase in settlement before the reinforcement becomes effective. These trends indicate that, from a practical design standpoint, geocell layers should be installed as close as possible to the footing base, while remaining within the zone of significant shear stresses.

Reinforcement width also exerted a clear influence on footing performance. At any given embedment depth, BCR increased with L/B, and the most pronounced improvement occurred when the width was increased from 2B to 3B. Further extension to 5B produced additional but progressively smaller gains, showing that beyond about three footing widths the benefits of extra reinforcement are subject to diminishing returns. This behavior suggests that an economical design may typically be achieved with a reinforcement width of L/B ≈ 3, while larger widths should be reserved for cases where maximizing bearing capacity is critical.

The geometry of the geocell proved to be equally important. Increasing the cell height from h/B = 0.5 to 1.0 (G2 to G1) resulted in BCR increases on the order of 30–50% at shallow embedment, confirming that taller cells provide deeper confinement and allow greater mobilization of bending and membrane resistance in the geocell mattress. Reducing the aperture ratio from z/B = 1.0 to 0.5 (G1 to G3) led to even more substantial improvements; the small-aperture, tall geocell G3 consistently produced the highest BCR values across all depths and widths. This demonstrates that geometries offering stronger lateral restraint and more effective interlocking with the sand are particularly advantageous for saturated granular foundations.

In summary, the study confirms that geocell reinforcement is an efficient and robust technique for enhancing the bearing capacity and serviceability performance of strip footings on saturated sand. For conditions similar to those examined, the results indicate that an optimal configuration consists of a relatively tall geocell (h/B ≈ 1) with small apertures (z/B ≈ 0.5), placed at a shallow depth (u/B ≈ 0.25) and extended laterally to at least three times the footing width (L/B ≥ 3). Future work could extend these findings to different soil types, loading regimes (e.g. cyclic or repeated loads), and multi-layer reinforcement arrangements, as well as to calibrated numerical analyses aimed at developing design charts and guidelines for geocell-reinforced shallow foundations.

Authors' Contributions

Authors contributed equally to this article.

Declaration

In order to correct and improve the academic writing of our paper, we have used the language model ChatGPT.

Transparency Statement

Data are available for research purposes upon reasonable request to the corresponding author.

Acknowledgments

We would like to express our gratitude to all individuals helped us to do the project.

Declaration of Interest

The authors report no conflict of interest.

Funding

According to the authors, this article has no financial support.

Ethics Considerations

In this research, ethical standards including obtaining informed consent, ensuring privacy and confidentiality were considered.

References

Binquet, J., & Lee, K. L. (1975). Bearing capacity tests on reinforced earth slabs. *Journal of the Geotechnical Engineering Division, ASCE*, *101*(12), 1241-1255. https://doi.org/10.1061/AJGEB6.0000219

Chen, P., Chen, Z., Guo, Z., Wang, T., & Yang, W. (2025). Experimental studies on the axial compression performance and bearing capacity of pultruded GFRP tube-concrete-round steel tube double-skin hollow columns.

Chen, Q., & Abu-Farsakh, M. (2015). Ultimate bearing capacity analysis of strip footings on reinforced soil foundation. *Soils and Foundations*, *55*(1), 74-85. https://doi.org/10.1016/j.sandf.2015.01.005

Dash, S. K. (2010). Influence of relative density of soil on performance of geocell-reinforced sand foundations. *Journal of Materials in Civil Engineering, ASCE*, *22*(5), 533-538. https://doi.org/10.1061/(ASCE)MT.1943-5533.0000040

Dash, S. K., Krishnaswamy, N. R., & Rajagopal, K. (2001a). Bearing capacity of strip footings supported on geocell-reinforced sand. *Geotextiles and Geomembranes*, *19*(4), 235-256. https://doi.org/10.1016/S0266-1144(01)00006-1

Dash, S. K., Krishnaswamy, N. R., & Rajagopal, K. (2001b). Strip footing on geocell-reinforced sand beds with additional planar reinforcement. *Geotextiles and Geomembranes*, *19*(8), 529-538. https://doi.org/10.1016/S0266-1144(01)00022-X

Fragaszy, R. J., & Lawton, E. (1984). Bearing capacity of reinforced sand subgrades. *Journal of Geotechnical Engineering, ASCE*, *110*(10), 1500-1507. https://doi.org/10.1061/(ASCE)0733-9410(1984)110:10(1500)

Huang, C. C. (2016). Ultimate bearing capacity of saturated reinforced horizontal ground. *Geosynthetics International*, *23*(1), 1-8. https://doi.org/10.1680/jgein.15.00027

Huang, C. C., & Tatsuoka, F. (1990). Bearing capacity of reinforced horizontal sandy ground. *Geotextiles and Geomembranes*, *9*(1), 51-82. https://doi.org/10.1016/0266-1144(90)90005-W

Moghaddas Tafreshi, S. N., & Dawson, A. R. (2010). Comparison of bearing capacity of a strip footing on sand with geocell and with planar forms of geotextile reinforcement. *Geotextiles and Geomembranes*, *28*(1), 72-84. https://doi.org/10.1016/j.geotexmem.2009.09.003

Najjar, M., Indraganti, M., & Furlan, R. (2025). The Role of Building Geometry in Urban Heat Islands: Case of Doha, Qatar. *Designs*, *9*(3), 77. https://doi.org/10.3390/designs9030077

Pokharel, S. K., Han, J., Leshchinsky, D., Parsons, R. L., & Halahmi, I. (2010). Investigation of factors influencing behavior of single geocell-reinforced bases under static loading. *Geotextiles and Geomembranes*, *28*(6), 570-578. https://doi.org/10.1016/j.geotexmem.2010.06.002

Shin, E. C., & Das, B. M. (2000). Experimental study of bearing capacity of a strip foundation on geogrid-reinforced sand. *Geosynthetics International*, *7*(1), 59-71. https://doi.org/10.1680/gein.7.0166

Terzaghi, K. (1943). *Theoretical Soil Mechanics*. John Wiley & Sons. https://doi.org/10.1002/9780470172766

Tianzheng, F., Clara Saracho, A., & Haigh, S. K. (2023). Microbially induced carbonate precipitation (MICP) for soil strengthening: A comprehensive review. *Biogeotechnics*. https://doi.org/10.1016/j.bgtech.2023.100002

Wang, K. D., Wu, S. F., & Chu, J. (2023). Mitigation of soil liquefaction using microbial technology: An overview. *Biogeotechnics*, *1*(1). https://doi.org/10.1016/j.bgtech.2023.100005